Measurement of friction in galling testing – an example of its use in characterising the galling behaviour of hardfacings at ambient and elevated temperature

J. Daure[1,*], M.J. Carrington[1], D.G. McCartney[1], D.A. Stewart[2], P.H. Shipway[1]

[1]Faculty of Engineering, University of Nottingham, UK

[2]Rolls-Royce plc, Derby, UK

*Corresponding author

Abstract

Galling is a category of severe adhesive wear that is defined by surface damage arising between sliding solids, distinguished by macroscopic, usually localized, roughening and creation of protrusions above the original surface. The identification of galling is through a visual observation of the tested surface and is therefore inherently subjective. Due to the microscopic processes behind the onset of galling being poorly understood, further work is needed to understand the behaviour of different materials under galling conditions, both at room temperature and elevated temperature.

The current paper describes the development of a new galling testing apparatus, broadly under the ASTM G196 configuration with the addition of in-situ torque measurements and an automated worm drive for sample rotation as well as band heaters allowing tests at elevated temperatures up to a maximum applied stress of 950 MPa. Results from galling tests conducted at room temperate and 300 °C for both Stellite 6 (Co-based) and Tristelle 5183 (Fe-based) hardfacings are presented.

The results show that the galling resistance of Tristelle 5183 is significantly reduced at elevated temperature (<52.8 MPa) compared to room temperature (158.3 MPa). In the case of Stellite 6, galling was not observed at either room temperature or 300 °C up to the maximum tested stress of 950 MPa.

Keywords:

Galling; tribotesting; galling stress; hardfacing; torque measurement

1 Introduction

Whilst galling is a common failure mode of materials in sliding contact, the causes and mechanisms behind it are poorly understood [1]. Galling is a form of severe adhesive wear that is defined by the ASTM committee G02 on wear and erosion in Standard G40 as, "*a form of surface damage arising between sliding solids, distinguished by macroscopic, usually localized, roughening and creation of protrusions above the original surface*" [2]. It can occur on one or both mating surfaces and, by definition (as described in the ASTM standard), must be visible by the human eye. However, adhesive deformation leading to surface roughening on the microscale is often referred to as incipient galling [3, 4]. It is recognised that galling shares many of the features of other forms of wear (such as adhesive

wear) but (to directly quote Budinski and Budinski [4]) "*The feature of galling that sets itself apart from other forms of wear is the severity and size of protrusions from the original surface that form during the rubbing process.*"

Galling is undesirable and often expensive to remedy within an industrial setting as it can lead to the total failure of components. It results in material being raised from the surface which impedes sliding against other surfaces and in severe cases can result in cold welding of mated components leading to seizure [3, 4].

Any situation with metals in sliding contact can suffer from galling, with the tendency to gall depending upon (amongst other things) the material types and applied load borne by the contact. Examples of situations that regularly suffer from galling issues include the sheet metal stamping industry, industries that use highly loaded threaded fasteners, applications which cannot adequately lubricate sliding surfaces due to contamination problems (such as sanitary systems, food processing, medical devices, nuclear reactors etc.) and the nuclear industry (valves) [1, 4-7]. Factors that have been suggested to affect the galling behaviour of a mating pair are: material composition, crystal structure, surface morphology, hardness, temperature, sliding speed, sliding distance, surface oxides and stacking fault energy [1, 4, 8-12]. Due to the range of factors that can affect the galling behaviour of a mating pair, there is no single stress level at which the wear behaviour definitively changes to galling; instead, the galling frequency of a material is said to increase with increasing stress [3].

Two of the most common laboratory galling test methods are those described in the ASTM standards G98 and G196 [13-15]. The most widely used galling test is the ASTM G98 Standard Test Method for Galling Resistance of Materials; this method uses button-on-block contact conditions in which a solid pin of Ø12.7 mm is rotated against a stationary block [14]. Although this method is widely used, results of galling stress can vary significantly between investigators [3, 12]. Hummel et al. [12] also found that the lowest galling stress can be over five times smaller than the highest non-galling stress for 303 stainless steel. It is suggested that the principal reason for this is that the identification of whether galling has occurred has no quantitative definition and is therefore inherently subjective. Additionally, the ASTM G98 standard does not specify the size of the corner radius of the button specimen; some users may remove the burrs on the edge of the sample whilst others may leave it sharp which can lead to differences in results from different users [3]. Waite et al. showed that the stress concentration increased as the corner radius was decreased and that the location of the stress concentration occurs at the point of maximum sliding distance (maximum radial distance) as shown in Figure 1 [16]. The combination of maximum sliding distance and the stress concentration as well as the area of zero tangential velocity at the centre of the rotating button results in galling typically occurring at the edge of the sample [3].

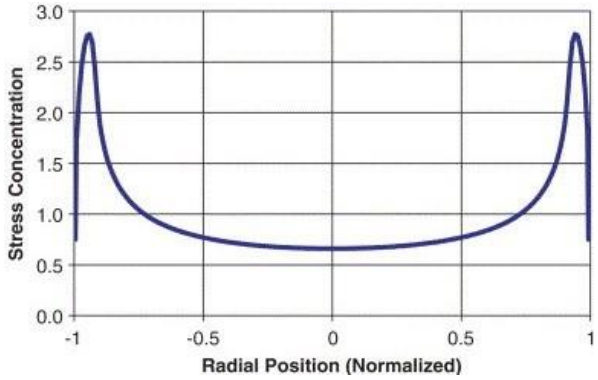

Figure 1 Plot of stress concentration factor versus normalized radial position along the diameter of a G98 galling pin with a 1.3 mm corner radius [16]

The ASTM G196 test method was developed by Hummel [3] to circumvent the issues associated with the ASTM G98 method. The testing configuration utilises two hollow cylinders which are mated resulting in a contact in the shape of an annulus [3]. The hole in the centre of the samples removes the point of zero velocity and an alignment pin is located in the centre of the samples which results in greater alignment throughout the test. The stress concentration is also said to be more evenly distributed across the contacting faces [3]. However, the ASTM G196 test method requires a large number of tests to be conducted and is therefore often expensive. Although the ASTM G196 is an improved test method for determining the galling behaviour of a material compared to ASTM G98, it still relies on the judgement of the investigator as to whether the material has galled. The rotation of the sample is also typically driven by hand (although automated sample rotation is allowed for in the standard) which can result in inconsistent sliding speeds, sliding distance and (commonly) stop and start events during rotation for sample re-gripping.

The main aim of this paper is to demonstrate the value of torque/friction measurements in characterising galling behaviour of representative hardfacing alloys at room temperature and at 300 °C in air using a modified G196 galling test rig which facilitates the uninterrupted and steady rotation of test samples under very high normal loads (up to 90 kN). One of the hardfacing alloys selected for study was the cobalt-based alloy Stellite 6 which is known for its excellent wear and galling resistance [9]. Stellite 6 has been traditionally used for nuclear power plant valves but due to the wear particles being transmuted to radioactive cobalt-60 in the reactor core, there is a need to replace this material in this environment [9]. The high galling resistance of Stellite 6 has been said to be due to its low stacking fault energy [17-21] which, under mechanical stress, promotes strain induced martensitic transformation and work hardening. This reportedly results in the formation of an easy-shear layer due to the transformation of the metastable face-centred cubic structure of the cobalt into a hexagonally close-packed (HCP) phase at the wear interface. The shear induced alignment of the hexagonal close-packed planes parallel to the sliding direction is said to improve galling resistance with the shear and adhesive transfer restricted to this layer. Studies on Stellite 6 at elevated temperature also show the formation of protective oxide layers which have been reported to be beneficial to its wear resistance [18, 20]. The other alloy selected was the iron-based alloy Tristelle 5183. High silicon stainless steels, such as the Tristelle family, have been introduced as potential lower cost alternatives to cobalt-based alloys for anti-galling applications [22].

2 Experimental procedure

2.1 Description of galling test rig

A test rig was developed in order to carry out galling tests under the ASTM G196 (Standard Test Method for Galling Resistance of Material Couples) [13] configuration. This method consists of two concentric hollow cylindrical specimens with their ends mated resulting in a contact area in the shape of an annulus. An alignment pin is located in the centre hole of the samples to ensure concentricity between the two specimens throughout the test. A schematic diagram of the G196 test configuration is presented in Figure 2.

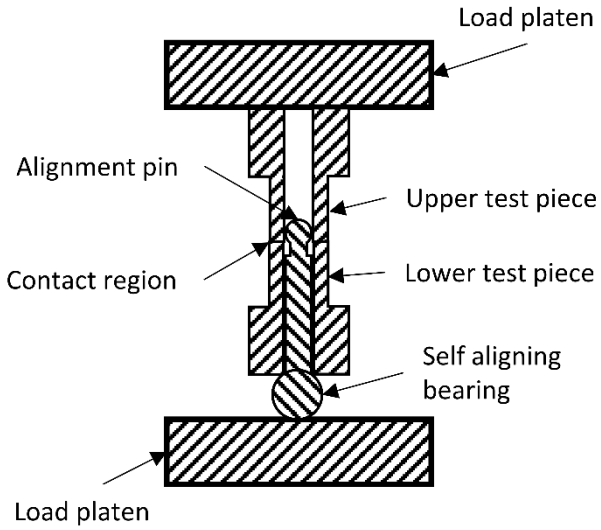

Figure 2 Schematic diagram showing a cross-sectional view of the test configuration. Loading is applied via the platens, the lower test piece remains stationary whilst the upper test piece is rotated through 360°.

A cross-sectional diagram of the test rig is presented in Figure 3. The rig conforms to a die-set configuration which is designed to fit into an Instron 5985 universal testing machine. The four support columns maintain alignment between the upper and lower sections of the rig. The base of the rig is fixed to the bed of the Instron machine and the upper section is attached to its load cell. Testing can be conducted up to a maximum normal load of 90 kN which, under the G196 sample dimensions, equates to a nominal contact pressure of 950 MPa.

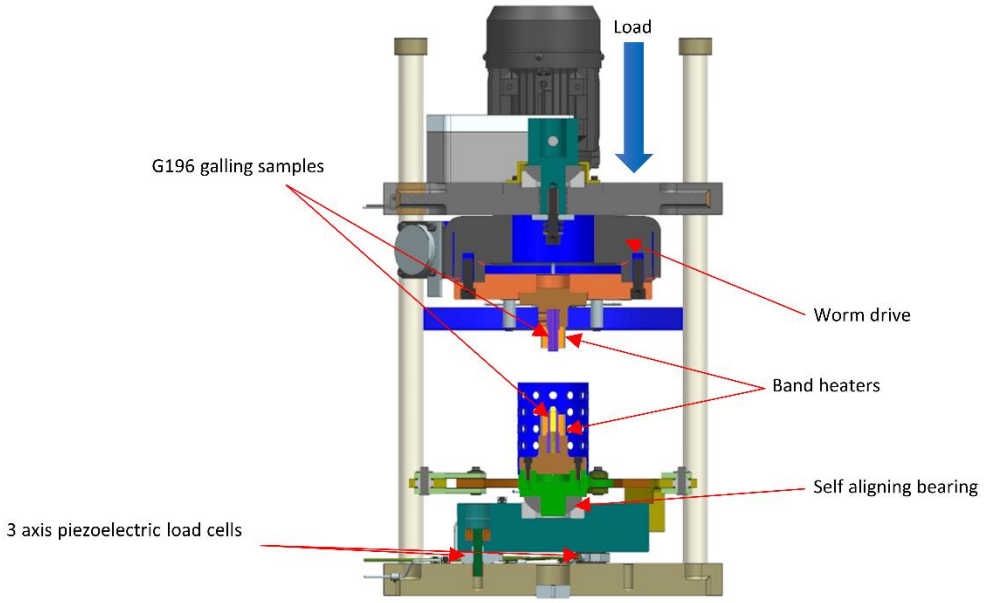

Figure 3 Schematic diagram showing a cross-sectional view of the of the galling test apparatus.

The use of an automated worm drive to rotate the upper test piece results in a constant and repeatable angular speed and distance for each test. A self-aligning bearing allows the transverse movement and angular displacement of the lower test piece whilst preventing any rotation about the central axis. This mechanism ensures repeatable pin alignment which results in symmetrical load distribution about the axis of rotation at the start of the test. This repeatable uniform loading is of paramount importance to high quality galling testing.

The test pieces are held in a chuck and secured by four grub screws which are screwed onto two flats on the base of the samples at 90° apart. The bottom chuck is fixed to the self-aligning bearing whilst the upper test piece is rotated through a single 360° turn per test. The continuous rotation of the test piece is conducted via a variable speed automated worm drive. For this work, the maximum speed setting was utilised which completes one full (360°) rotation in 14 seconds (~ 0.45 rad s^{-1}).

The vertical load and the torque are measured from the output of three sensitive 3-axis piezoelectric load cells (Kistler Instruments Ltd.) which are located under the base plate arranged at 120° apart; the sensitivity of the load cells is 8.1 pC N^{-1} for the shear force (torque) and 3.7 pC N^{-1} for the normal load. In this work, data were acquired at a sampling rate of 10 Hz.

Band heaters with copper bushings surround the test pieces which allow elevated temperature tests to be conducted with a maximum operating temperature of 700 °C. K-type thermocouples are inserted into machined slots in the copper bushings to constantly monitor and control the temperature of the heaters.

2.2 Materials and Test procedure

The alloys examined in this work were the Co-based hardfacing alloy Stellite 6 and Fe-based hardfacing alloy Tristelle 5183, both supplied by LSN Diffusion (Llandybie, UK), the compositions of which are

presented in Table 1. Both had been manufactured by hot isostatic pressing (HIPing) of gas atomised powder.

The test pieces are hollow cylinders of 50 mm length where the contacting face is Ø12.7 mm outer diameter (OD) and Ø 6.375 mm inner diameter (ID). Testing was conducted on samples with parallel ground surfaces giving them a surface roughness (Ra) of approximately 0.2 – 0.4 µm as measured by stylus profilometry on a sample disc by taking an average roughness from measurements taken in different directions along the sample. Prior to testing, any burrs were removed using 400 grit silicon carbide paper on the outer and inner diameter perpendicular to the test surface. The surfaces were then cleaned using cotton wool and ethanol.

Table 1 Compositions of alloys as determined by chemical analysis

	Element (wt%)									
Alloy	C	Co	Cr	Fe	N	Nb	Ni	Si	W	Other
Stellite 6	0.96	Bal.	27.08	0.73	-	-	0.87	1.47	5.01	0.07
Tristelle 5183	2.08	-	21.72	Bal.	0.05	6.90	10.39	4.67	-	0.73

The normal load was applied by an Instron 5985 testing machine operating in load-controlled mode. Tests were carried out from an initial normal load of 5 kN (52.8 MPa) for Tristelle 5183 and from 80 kN (844 MPa) for Stellite 6. After one full rotation, the samples were removed and inspected for galling characteristics. These characteristics included concentric striations of severe macroscale surface roughening where the grinding marks are no longer observed and/or cold welding of the two samples.

If galling had not occurred, testing was conducted on a new pair of samples at a load 5 or 10 kN greater than the previous load. This was repeated until signs of galling were observed. Once galling had occurred, repeat tests were conducted on new samples at 5 kN above and below the load at which galling was initially observed. In the instance that galling did not occur at the higher load, the test procedure was repeated until consistent galling was observed. For this work, a minimum of two tests were conducted at each load. Due to limited sample availability in the test programme, the ASTM G196 standard test method was not followed (the standard test method requires at least 48 tests to be conducted in order to determine a galling load).

When testing at the elevated temperature of 300 °C, the following procedure was followed to determine the temperature at the contacting surface. A wire thermocouple was placed between the two contacting surfaces of samples which were then brought into contact with an applied load less than 0.5 kN (<5.3 MPa). The band heater settings were adjusted until the measured temperature in the contact stabilised at 300 °C ± 5 °C. These band heater settings were then maintained for the galling tests with that material type (where no in-contact thermocouple was in place), with these settings being regularly re-checked.

2.3 Materials Characterisation

Microstructural characterisation was performed using optical microscopy, scanning electron microscopy (SEM) using secondary electron (SE) and backscattered electron (BSE) imaging and energy dispersive X-ray spectroscopy (EDX) analysis. The surface to be examined was progressively ground to a 1200 grit finish, diamond polished to a 1 µm finish and given a final polish using 0.06 µm colloidal silica. SEM was conducted using a Quanta 600 utilising a tungsten filament source and a 20 kV beam.

Following testing, visual examinations were made on the samples as well as stereoscopy of the tested surfaces.

Hardness measurements were performed on polished samples using a Vickers indenter and a 20 kg load. Ten indents were performed on each material and a mean hardness was calculated from these.

2.4 Analysis of torque data

Short term fluctuations in the measured torque in the galling tests were quantified by calculating the deviation of the raw data from smoothed data. The torque data were smoothed by Savitzky-Golay filtering using a 3rd degree polynomial and 25 data points. The absolute deviation from the smoothed torque was calculated for every point and an average was taken from all points recorded after two seconds into the test.

The coefficient of friction, μ, in an annular contact of this type is given by the following equation [23]:

$$\mu = \frac{3}{2}\frac{r_2^2 - r_1^2}{r_2^3 - r_1^3}\left(\frac{T}{F_a}\right) \quad (1)$$

where T is the torque, r_1 and r_2 are the inner and outer radii respectively of the contacting faces and F_a is the applied normal force. The specimen radii r_1 and r_2 (as per ASTM G196) are 3.1875 mm and 6.3500 mm respectively. Using these values, Equation 1 can be simplified to:

$$\mu = 202.3\left(\frac{T}{F_a}\right) \quad (2)$$

3 Results

3.1 Characterisation of hardfacing alloys

The hardnesses of the alloys were measured to be 368 ± 1 HV_{20} for Tristelle 5183 and 401 ± 3 HV_{20} for Stellite 6.

SEM-BSE micrographs of HIPed Stellite 6 are shown in Figure 4 (a & b) and reveal dark-contrast, equiaxed chromium-rich carbide precipitates (M_7C_3), ranging in size between ~ 1 and 5 µm, in a Co-rich matrix in which grain and annealing twin boundaries are clearly visible. Figure 4 (c & d) show BSE micrographs of Tristelle 5183 in which the bright-contrast precipitates are the NbC phase, the dark grey contrast precipitates (~ 1-2 µm in size) are the M_7C_3 phase and the lighter grey contrast matrix is principally a γ-Fe fcc matrix.. The matrix contrast variation arises from BSE channelling contrast and the presence of small amounts of α-Fe and π-ferrosilicide. The NbC has a bimodal size distribution with most of the precipitates being < 2 µm in size but a small number being up to ~ 5 – 20 µm in size (Figure

4 (c)). It has previously been shown [24] that the large NbC particles are formed during the alloying and melting of the material prior to gas atomisation of the melt. The resultant gas atomised powder is subsequently HIPed.

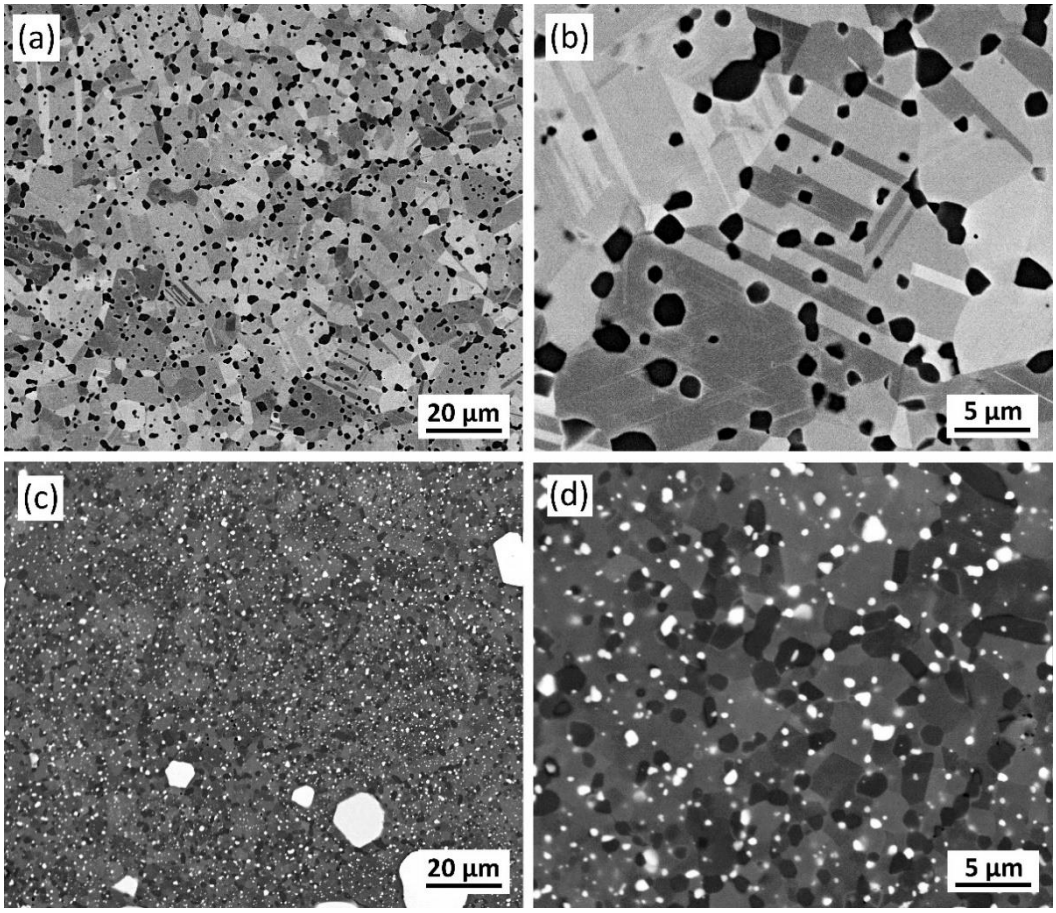

Figure 4 BSE SEM micrographs of polished HIPed materials as follows: (a & b) Stellite 6 showing a dark contrast M_7C_3 phase and a dark and light grey phase for the cobalt matrix as well as annealing twins; (c & d) Tristelle 5183 showing a bright contrast NbC phase, a dark grey M_7C_3 phase and a lighter grey matrix of varying contrast.

3.2 Galling test results

3.2.1 Observations of surface features

Representative optical microscope images of Tristelle 5183 samples tested at room temperature and 300 °C are presented in Figure 5. In these micrographs, galling is characterised by concentric striations of severe macroscale surface roughening where the grinding marks are no longer observed (indicated by the blue arrows). Dark areas, where the grinding marks are difficult to observe, are seen on some of the sample surfaces (indicated by red arrow). In these areas the surface was visibly polished to a near mirror finish during the galling testing. Due to the direct light from the stereo microscope, the polished areas reflect the light and appear dark when imaged such as observed in Figure 5 (b) (indicated by the red arrow).

At room temperature, surface polishing of Tristelle 5183 is observed at a load of 10 kN as evidenced by the darker surface of Figure 5 (b). In Figure 5 (a), other than some mild polishing in the top right section, the sample is largely unworn. At a load of 15 kN, further polishing is observed; however, adhesive deformation features appear to lie in the transition between galling initiation (microscale adhesion) and galling (Figure 5 (c & d)). Areas of concentric markings, consistent with microscale adhesion where the grinding marks are no longer visible, can be observed (as indicated by the blue arrows). This subjective interpretation of surface features highlights a fundamental limitation of the identification of galling by optical methods. At 20 kN (Figure 5 (e & f)), galling is clearly observed (as indicated by the blue arrow).

Galling can be observed in all tests on Tristelle 5183 at 300 °C, even at the lowest tested load of 5 kN as indicated by the blue arrow in Figure 5 (g). At each load, large areas of concentric deformation can be observed. With 10 and 15 kN loads, severe galling deformation is observed across the entire surface of one sample (Figure 5 (j & k)).

In some tests, the severity of wear can differ significantly across the sample surface such as in (Figure 5 (i & l). This is due to the stochastic nature of galling and can depend on the location and time from the start of the test at which the galling occurs.

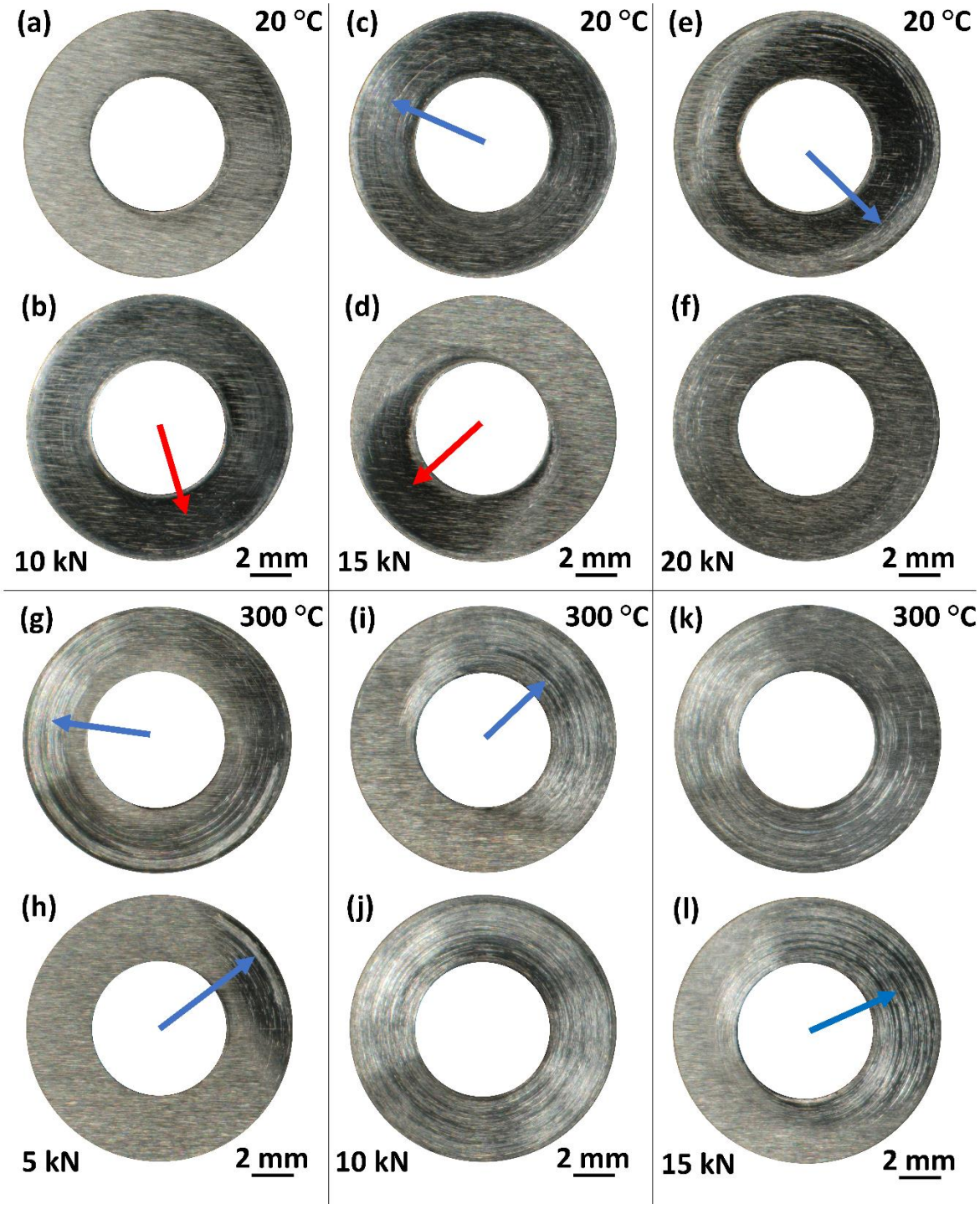

Figure 5 Stereo microscope images of surfaces of Tristelle 5183 following tests at room temperature and 300 °C under different loads (red arrow indicates surface polishing, blue arrows indicate galling behaviour).

Representative images of Stellite 6 samples tested at room temperature and 300 °C are presented in Figure 6. Galling was not observed on Stellite 6 samples at room temperature or at 300 °C up to the maximum tested load of 90 kN (950 MPa contact pressure). Significant amounts of surface polishing

are observed as evidenced by the dark surface features (which are highly reflective of incident light) covering the entire surfaces of room temperature tested samples and as indicated by red arrows on the 300 °C tested samples. A greater degree of localised surface polishing was observed at 300 °C (Figure 6 (e-h)) compared to room temperature (Figure 6 (a-d)). Although wear was inflicted on the surfaces, no areas of concentric striations or severe macroscale surface roughening were observed.

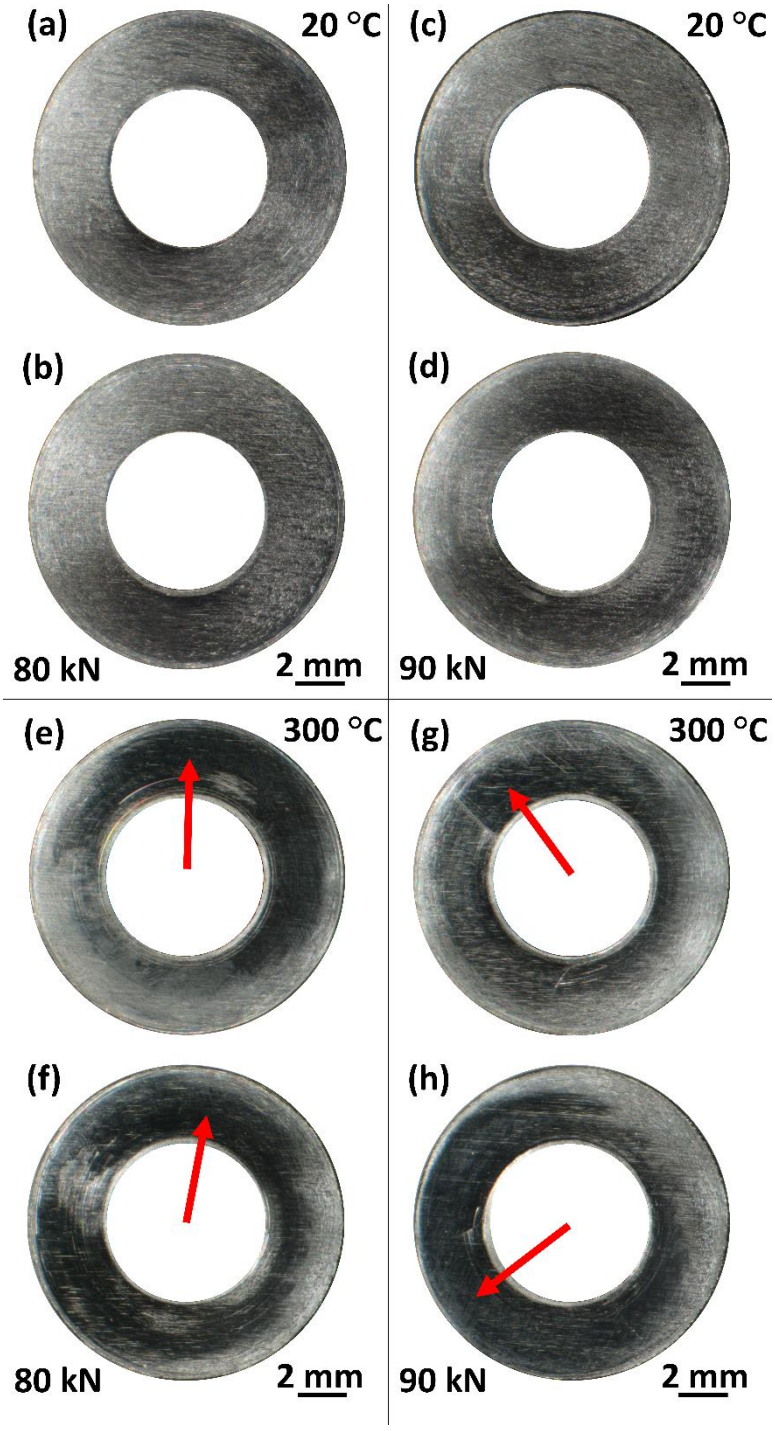

Figure 6 Stereo microscope images of tested Stellite 6 sample surfaces at room temperature and 300 °C; galling was not observed at the maximum tested load.

3.2.2 **Torque measurements**

Representative histories of torque versus sample rotation recorded during the galling testing of Tristelle 5183 at room temperature are presented in Figure 7, with the black lines representing the smoothed torque data. The torque is observed to increase with increasing normal load as expected. At 10 kN (i.e. below the galling load determined from optical examination of the surfaces following testing), the fluctuations in torque from the smoothed data appear to be smaller than those observed in tests at the higher normal loads that produced galling. It is postulated that these fluctuations relate to localised cold welding followed by fracture that occurs during the initiation of galling.

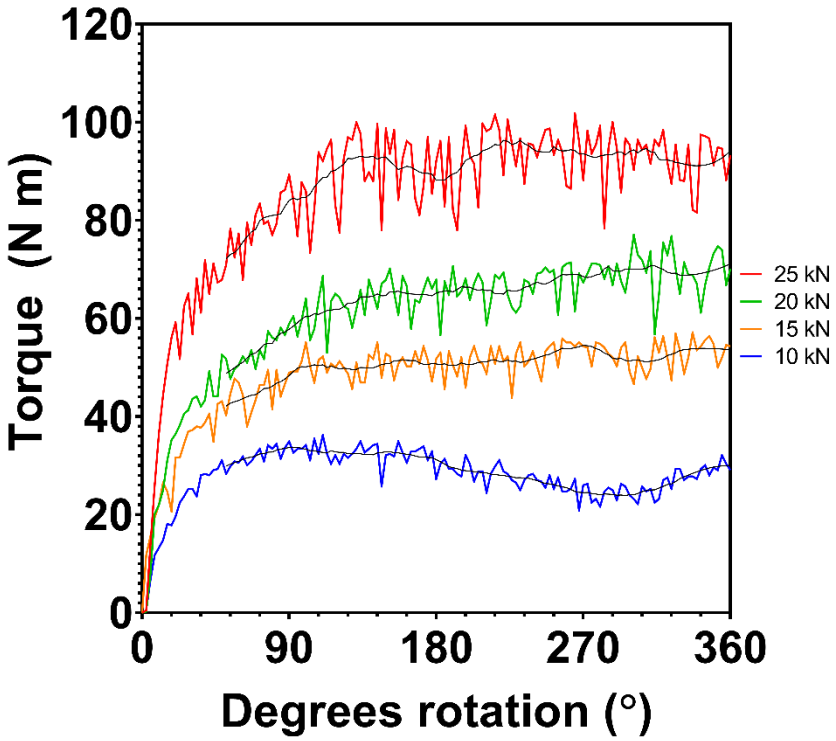

Figure 7 Variation of torque with sample rotation during galling tests on Tristelle 5183 at room temperature. Galling was not observed visually at 10 kN. The increase in galling observed correlates with an increase in deviation from the smoothed torque (black line).

To quantify these short-term torque fluctuations, the deviation from the smoothed torque was calculated at each point (from two seconds into the test and onwards) and an average deviation was calculated for each test. The results are presented in Table 2. A clear increase in average deviation from the smoothed torque is observed with increasing load at room temperature as the adhesive wear becomes more severe.

The torque histories for the galling tests on Tristelle 5183 at a normal load of 15 kN at both room temperature and 300 °C are presented in Figure 8. Tests at both temperatures resulted in macroscopic galling behaviour and little difference is observed in the maximum torque values. However, the rate of increase of torque was higher for the test conducted at 300 °C, possibly due to the more severe damage accumulation observed at elevated temperature. The average deviation from the smoothed torque was

significantly lower during the elevated temperature test (0.49 N m at 300 °C compared with 2.04 N m at room temperature), even though the adhesive behaviour was much more severe at the higher temperature. Unlike the room temperature behaviour, short term torque fluctuations in tests at 300 °C were found not to change with increasing load as shown in Table 2. This is believed to be due to a change in wear mechanisms at elevated temperature.

Table 2 Mean torque deviation from the smoothed torque data for Tristelle 5183 at room temperature and 300 °C

Load (kN)	Mean deviation in torque from the smoothed data Room temp (N m)	Mean deviation in torque from the smoothed data 300 °C (N m)
5	-	0.56
10	1.35	0.45
15	2.04	0.49
20	2.44	-
25	4.44	-

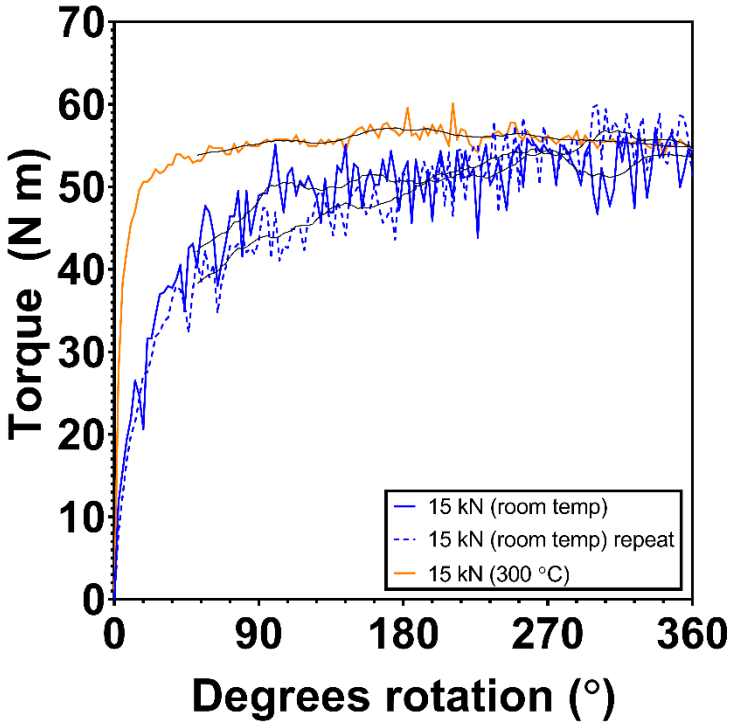

Figure 8 Variation of torque with sample rotation during galling tests on Tristelle 5183 under 15 kN load at room temperature and at 300 °C. The room temperature test resulted in some adhesive behaviour whilst severe galling was observed at 300 °C. Black lines represent the smoothed torque.

The torque results for Stellite 6 tested at 80 kN and 90 kN (at both room temperature and 300 °C) are presented in Figure 9 (a & b) respectively. Galling was not observed in any of these tests but the torque was significantly lower when tested at elevated temperature at both loads. Tests at room temperature also revealed an initial maximum in the torque followed by a gradual decline throughout the test, whereas at 300 °C the torque generally remained constant following the initial increase. The torque was seen to increase with load at room temperature, however, at 300 °C the torque showed little change with increasing load.

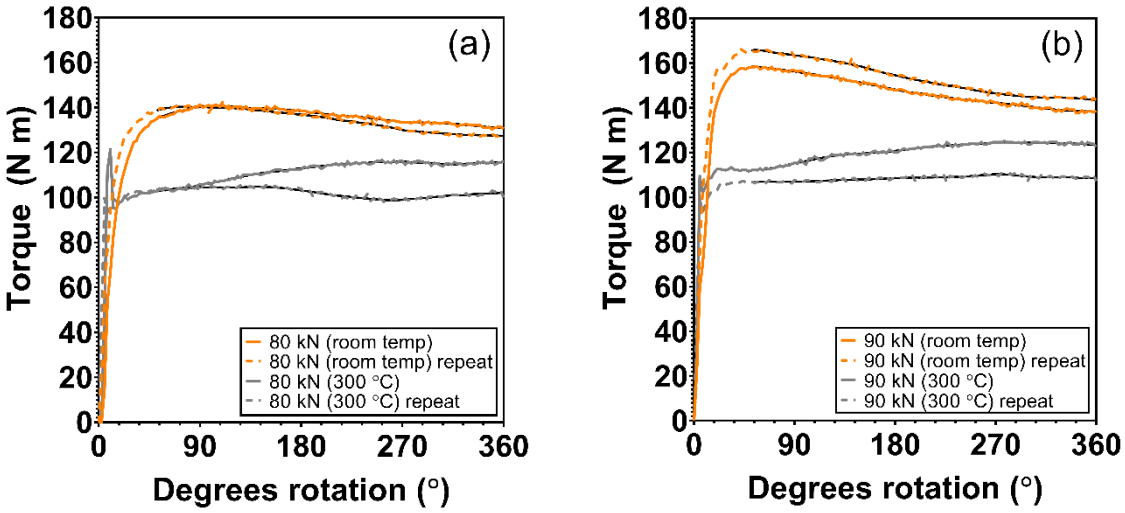

Figure 9 Variation of torque with sample rotation during galling tests on Stellite 6 under (a) 80 kN load and (b) 90 kN load at both room temperature and 300 °C. Galling was not observed visually in these tests. Black lines represent the smoothed torque.

The average deviation from the smoothed torque for Stellite 6 tested at 80 and 90 kN are presented for room temperature and elevated temperature in Table 3. Stellite 6 exhibited a similar average deviation for both temperatures.

Table 3 Mean torque deviation from the smoothed torque data for Stellite 6 at room temperature and 300 °C.

Load (kN)	Mean deviation in torque from the smoothed data Room temp (N m)	Mean deviation in torque from the smoothed 300 °C (N m)
80	0.40	0.43
90	0.46	0.44

4 Discussion

4.1 Coefficient of friction

In order to compare the torque results for Stellite 6 and Tristelle 5183, the results of friction coefficient (calculated from equation 2) for Tristelle 5183 at 10 kN and Stellite 6 at 90 kN (room temperature and 300 °C) are presented in Figure 10. It is clear from duplicate tests that the repeatability is good for Stellite 6. Despite the spread in results for Tristelle 5183, the alloys show distinctly different galling

behaviour. Therefore, although galling is stochastic in nature, the use of an automated motor to turn the samples at a constant speed offers an improvement over the ASTM G196 standard which allows samples to be turned by hand as well as allowing stopping to re-grip the turning tool.

The friction coefficient for Tristelle 5183, tested at 10 kN, increased at elevated temperature which is expected due to the greater amount of damage inflicted on the material at 300 °C. Galling was not observed in the room temperature tests but was observed in the test carried out at 300 °C.

Stellite 6 was not observed to exhibit galling behaviour at any of the loads employed in the tests. Interestingly, the torque and friction coefficient for Stellite 6 was lower when tested at 300 °C compared to room temperature for both 80 kN and 90 kN tests. The friction coefficient for Stellite 6 tested at 90 kN was also significantly lower than that of Tristelle 5183 tested at 10 kN at both room temperature and 300 °C. This could be expected since Stellite 6 is well-known for its low friction behaviour and resistance to galling [18, 19].

The torque traces for Stellite 6 also exhibited smoother curves, with fewer short-term fluctuations confirming the lack of adhesive behaviour compared to Tristelle 5183. The friction coefficients for Stellite 6 tested at 80 kN were almost identical to those observed during tests at 90 kN at both temperatures.

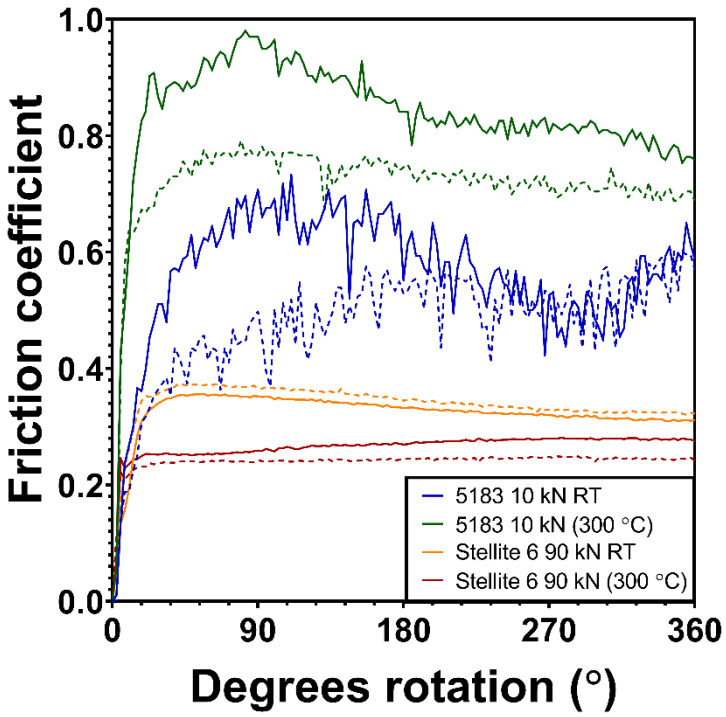

Figure 10 Variation of friction coefficient with sample rotation during galling tests on 5183 under 10 kN load and Stellite 6 under 90 kN load at room temperature and 300 °C. Galling of Tristelle 5183 was not observed at room temperature but was observed at 300 °C. Galling was not observed on Stellite 6 at either temperature. Dashed lines represent duplicate tests

The coefficient of friction data presented in Figure 10 show that torque measurements, when combined with an automated worm drive to rotate samples at a constant speed, can be very useful, both in identifying the presence of adhesive wear and also in characterising the behaviour of the material during galling testing. The differences observed in wear behaviour of the two materials and also of each material at the different temperatures would not have been so clearly evident if conducting the sample rotation by hand due to inconsistencies in applied rotational speeds and stop-start events.

The torque revealed a clear lack of adhesive behaviour on Stellite 6 even at the maximum tested load of 90 kN (950 MPa), whereas Tristelle 5183 exhibited clear adhesive behaviour in most tests. A change in behaviour was observed on both materials at 300 °C, but further work needs to be carried out to understand this change in wear mechanisms at elevated temperature.

4.2 Behaviour of Tristelle 5183

Tristelle 5183 exhibited galling behaviour from normal loads of 15 kN (158.3 MPa) at room temperature and from the lowest tested normal load of 5 kN (52.3 MPa) at 300 °C. This reduction in galling resistance at elevated temperature could be due to the softening of the material at higher temperate or due to an increase in stacking fault energy which decreases the tendency for the fcc matrix to undergo a deformation induced martensitic transformation [25-28]. This could also explain the smaller short-term torque fluctuations observed at elevated temperature but more work needs to be conducted on this aspect to further understand the effects of temperature on the galling behaviour of this iron-based alloy.

Although short-term torque fluctuations were lower at 300 °C for Tristelle 5183, a higher maximum torque was observed during 10 kN tests at 300 °C compared to those at room temperature, with this being expected due to the increase in galling and adhesive wear at elevated temperature. When tested at 15 kN, in which galling behaviour was observed at both room temperature and 300 °C, the maximum torque reached was similar at both temperatures.

At room temperature, an increase in short term torque fluctuations with increasing load and therefore increasing adhesive behaviour was observed. This is likely to be caused by the formation and breaking of adhesive bonds that takes place during adhesive wear and galling and demonstrates the value of torque measurements in identification of the occurrence of galling.

4.3 Behaviour of Stellite 6

No galling was observed on Stellite 6 up to the maximum tested load of 90 kN (950 MPa) at both room temperature and 300 °C. The impressive wear resistance of Stellite 6 is not fully understood, however, a large amount of literature has been published on this subject. One of the most common proposed reasons for the wear behaviour of Stellite 6 is due to its low stacking fault energy which promotes strain induced martensitic transformation and work hardening resulting in the formation of an easy-shear layer at the wear interface [17-21]. It is expected that this is occurring on the contacting surfaces under the testing conditions investigated, however, further work is needed to investigate this.

Stellite 6 exhibited surface polishing at both temperatures, with an increase in surface polishing observed at 300 °C. A lower torque was also observed for tests conducted at 300 °C; this may be due

to the formation of protective oxide layers or a change in stacking fault energy [18, 20], however, further work needs to be conducted to investigate this. For the purpose of this paper, the focus is to demonstrate the value of torque measurements in galling to reveal these differences in behaviour that would otherwise not be apparent under the current ASTM G196 test method.

Large short-term torque deviations were not observed for Stellite 6 at both test temperatures which suggests a lack of adhesive behaviour.

5 Conclusions

- An improved galling rig was developed to perform tests under the ASTM G196 configuration. It employs an automated worm drive to rotate the sample at a constant angular speed (0.45 rad/s) over a fixed rotation (2π radians, i.e. 360°) whilst measuring the frictional torque throughout the test.

- Repeatable galling testing can be conducted under the ASTM G196 configuration up to high contact pressures of 950 MPa through the use of a mechanical drive.

- Measurement of torque provides information as to the evolution of coefficient of friction during individual galling tests; such information is not available from tests which are not instrumented in this way.

- The torque, combined with automated sample rotation at a constant speed, has been shown to help identify the presence of adhesive wear and changes in deformation behaviour for different materials and different temperatures.

- The changes in torque reveal a change in frictional / deformation behaviour, for both materials, at elevated temperature as witnessed by the differences in friction coefficient and torque fluctuations.

- The galling resistance of Tristelle 5183 was significantly lowered when tested at 300 °C whereas there was no evidence of galling in Stellite 6 up to the maximum tested load of 90 kN (950 MPa) at both room temperature and 300 °C. Additionally, Stellite 6 exhibits a lower friction coefficient at elevated temperature than at room temperature.

Acknowledgements

The authors would like to thank CNR Services International Ltd., Nottingham, UK. for the design and build of the galling rig and supplying the schematic in Figure 3. The authors gratefully acknowledge funding from Rolls-Royce plc. M.J. Carrington also acknowledges funding from the Faculty of Engineering, University of Nottingham in support of a PhD studentship. The authors would also like the thank the Nanoscale and Microscale Research Centre (nmRC) at the University of Nottingham for providing access to their instrumentation.

References

[1]. Daure, J.L., M.J. Carrington, P.H. Shipway, D.G. McCartney, and D.A. Stewart, *A comparison of the galling wear behaviour of PVD Cr and electroplated hard Cr thin films.* Surface and Coatings Technology, 2018. **350**: p. 40-47.

[2]. ASTM, *G40-17 Standard Terminology Relating to Wear and Erosion*. 2017.

[3]. Hummel, S.R., *Development of a galling resistance test method with a uniform stress distribution.* Tribology International, 2008. **41**(3): p. 175-180.

[4]. Budinski, K.G. and S.T. Budinski, *Interpretation of galling tests.* Wear, 2015. **332-333**: p. 1185-1192.

[5]. Eriksson, J. and M. Olsson, *Tribological testing of commercial CrN, (Ti,Al)N and CrC/C PVD coatings - Evaluation of galling and wear characteristics against different high strength steels.* Surface & Coatings Technology, 2011. **205**(16): p. 4045-4051.

[6]. Karlsson, P., A. Gåård, P. Krakhmalev, and J. Bergström, *Galling resistance and wear mechanisms for cold-work tool steels in lubricated sliding against high strength stainless steel sheets.* Wear, 2012. **286-287**: p. 92-97.

[7]. Voss, B.M., M.P. Pereira, B.F. Rolfe, and M.C. Doolan, *A new methodology for measuring galling wear severity in high strength steels.* Wear, 2017. **390-391**: p. 334-345.

[8]. Harsha, A.P., P.K. Limaye, R. Tyagi, and A. Gupta, *Effect of Temperature on Galling Behavior of SS 316, 316 L and 416 Under Self-Mated Condition.* Journal of Materials Engineering and Performance, 2016. **25**(11): p. 4980-4987.

[9]. Vikström, J., *Galling resistance of hardfacing alloys replacing Stellite.* Wear, 1994. **179**(1): p. 143-146.

[10]. Barzdajn, B., A.T. Paxton, D. Stewart, and F.P.E. Dunne, *A crystal plasticity assessment of normally-loaded sliding contact in rough surfaces and galling.* Journal of the Mechanics and Physics of Solids, 2018. **121**: p. 517-542.

[11]. Hummel, S.R., *New test method and apparatus for measuring galling resistance.* Tribology International, 2001. **34**(9): p. 593-597.

[12]. Hummel, S.R. and B. Partlow, *Comparison of threshold galling results from two testing methods.* Tribology International, 2004. **37**(4): p. 291-295.

[13]. ASTM, *G196-08(2016) Standard Test Method for Galling Resistance of Material Couples*. 2016, ASTM International: West Conshohocken, PA.

[14]. Hummel, S.R. and J. Helm, *Galling50, a Stochastic Measure of Galling Resistance.* Journal of Tribology, 2009. **131**(3).

[15]. ASTM, *G98-17 Standard Test Method for Galling Resistance of Materials*. 2017, ASTM International: West Conshohocken, PA.

[16]. Waite, R.A., S.R. Hummel, A. Herr, and G. Dalton, *Analysis of the stress field in a threshold-galling test.* Tribology International, 2006. **39**(11): p. 1421-1427.

[17]. Cross, P.S.G., G. Limbert, D. Stewart, and R.J.K. Wood, *Ratcheting wear of a cobalt-chromium alloy during reciprocated self-mated dry sliding.* Wear, 2019. **426-427**: p. 1142-1151.

[18]. Wood, P.D., H.E. Evans, and C.B. Ponton, *Investigation into the wear behaviour of Stellite 6 during rotation as an unlubricated bearing at 600°C.* Tribology International, 2011. **44**(12): p. 1589-1597.

[19]. Persson, D.H.E., E. Coronel, S. Jacobson, and S. Hogmark, *Surface analysis of laser cladded Stellite exposed to self-mated high load dry sliding.* Wear, 2006. **261**(1): p. 96-100.

[20]. Kashani, H., A. Amadeh, and A. Ohadizadeh, *Effect of temperature on the strain induced $\gamma \rightarrow \varepsilon$ phase transformation in Stellite 21 during wear test.* Materials Science and Engineering: A, 2006. **435–436**: p. 474-477.

[21]. Bhansali, K.J. and A.E. Miller, *The role of stacking fault energy on galling and wear behavior.* Wear, 1982. **75**(2): p. 241-252.
[22]. Mellor, B.G., *Surface Coatings for Protection Against Wear*. 2006, Cambridge: Woodhead Publishing.
[23]. Singh, S., *Theory of Machines*. 2013: Pearson Education India.
[24]. Carrington, M.J., J. Daure, V.L. Ratia, P.H. Shipway, D.G. McCartney, and D.A. Stewart, *Microstructural characterisation of Tristelle 5183 (Fe-21%Cr-10%Ni-7.5%Nb-5%Si-2%C in wt%) alloy powder produced by gas atomisation.* Materials & Design, 2019. **164**: p. 107548.
[25]. Molnár, D., X. Sun, S. Lu, W. Li, G. Engberg, and L. Vitos, *Effect of temperature on the stacking fault energy and deformation behaviour in 316L austenitic stainless steel.* Materials Science and Engineering: A, 2019. **759**: p. 490-497.
[26]. Remy, L. and A. Pineau, *Twinning and strain-induced F.C.C. → H.C.P. transformation in the Fe・Mn・Cr・C system.* Materials Science and Engineering, 1977. **28**(1): p. 99-107.
[27]. Pierce, D.T., J.A. Jiménez, J. Bentley, D. Raabe, and J.E. Wittig, *The influence of stacking fault energy on the microstructural and strain-hardening evolution of Fe–Mn–Al–Si steels during tensile deformation.* Acta Materialia, 2015. **100**: p. 178-190.
[28]. Mosecker, L., D.T. Pierce, A. Schwedt, M. Beighmohamadi, J. Mayer, W. Bleck, and J.E. Wittig, *Temperature effect on deformation mechanisms and mechanical properties of a high manganese C+N alloyed austenitic stainless steel.* Materials Science and Engineering: A, 2015. **642**: p. 71-83.